

Proceedings of the Korean Nuclear Society Spring Meeting
Gyeongju, Korea, May 2003

Conceptual Design of Axial Flow Gas Turbines for Helium-cooled Reactors

Ji Hwan Kim, Hyeun Min Kim and Hee Cheon NO

Korea Advanced Institute of Science and Technology
Yuseong-Gu, Daejeon, Korea 305-701
Tel:+82-42-869-3857, Fax:+82-42-869-3895, Email:espero@.kaist.ac.kr

Abstract

The conceptual design tools for axial flow gas turbines were developed using mean-line analysis and meridional flow analysis methods. And it is validated by comparing with the turbomachinery design data of MPBR designed by the industry design tool. The conceptual design tools have ability to produce design point performance within the range of $\pm 1\%$ error comparing with the reference. It turns out that the high-pressure compressor and the high-pressure turbine consist of 8 stages and 4 stages. The analysis of the off-design of gas turbines show that constant speed lines are not steep as the mass flow increases mainly due to the high sonic velocity of helium and low flow coefficient, and the efficiency of the high-pressure is relatively constant over the wide range of pressure ratio. The results of the scaling analysis with 1/2 scale-down gas turbines indicate that the effects of the non-dimensional mass flow and the non-dimensional speed are stronger than the effect of the Reynolds number in subsonic flow regime.

1. Introduction

Gas turbines are generally considered as power conversion system for gas-cooled reactors, and the design of gas turbines needs highly advanced technology and much experience. The development of gas-cooled reactor system is being carried out in several countries for its benefits in performance and design simplicity, and so on. The closed cycle is under consideration for the energy-conversion process because of using the nuclear heat sources and the helium gas as a working fluid. Additionally the closed cycle has benefit to use a high pressure throughout the system, thus the size of turbomachinery can be reduced for a given power. In comparison with air the specific heat of helium is high, thus the gas turbine requires more stages to achieve the given temperature ratio. In spite of

2. Theory of Axial Flow Gas Turbines

2.1 Basic Theory

From the Euler's equation and velocity diagrams [1], the stagnation temperature rise in the compressor stage, ΔT_{oS} , is given by

$$\Delta T_{oS} = T_{o3} - T_{o1} = T_{o2} - T_{o1} = \frac{UC_a}{C_p} (\tan \mathbf{b}_1 - \tan \mathbf{b}_2) \quad (2.1)$$

Similarly, Euler's equation and the velocity diagrams in the turbine stage yield

$$W = \dot{m}UC_a (\tan \mathbf{a}_2 + \tan \mathbf{a}_3) = \dot{m}UC_a (\tan \mathbf{b}_2 + \tan \mathbf{b}_3) \quad (2.2)$$

Figures 2.1 and 2.2 show the cross-sectional view of the typical compressor and the turbine stages.

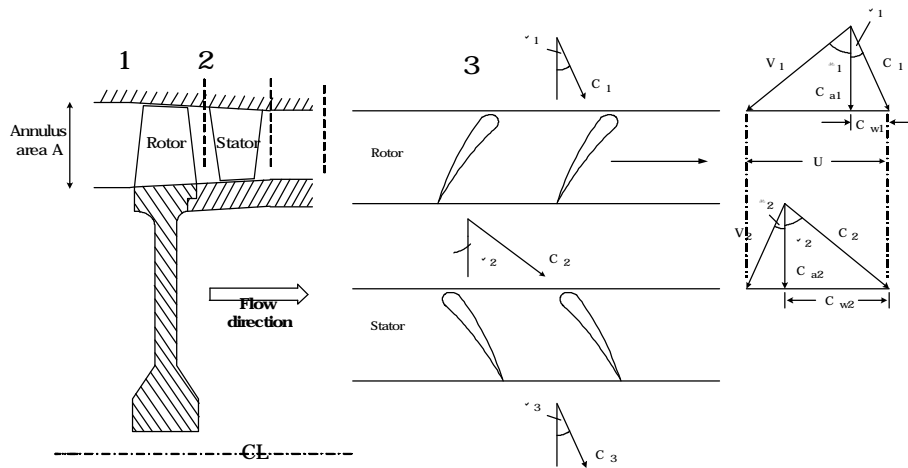


Figure. 2.1 A typical axial flow compressor stage

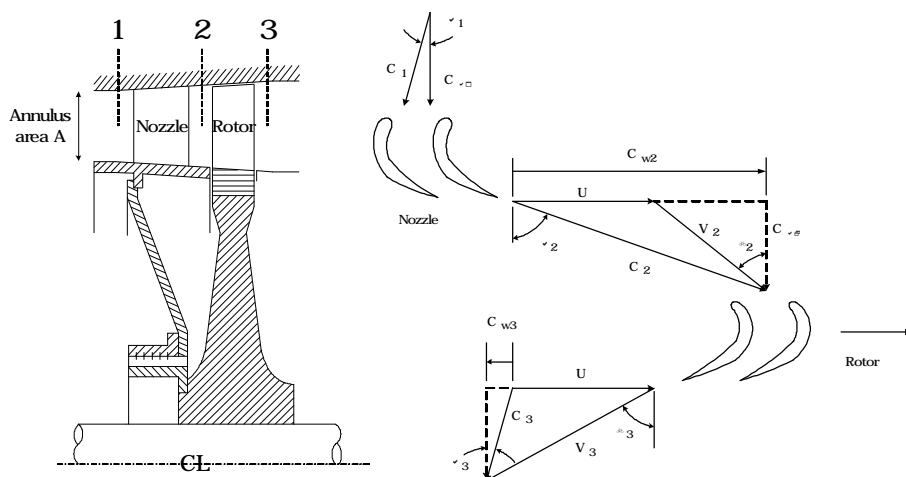


Figure. 2.2 A typical axial flow turbine stage

2.2 Radial Equilibrium Equation for Compressors

From the radial equilibrium equation and the definition of the stagnation enthalpy, the variation of enthalpy with radius is given by the following equation:

$$\frac{dh_o}{dr} = \frac{dh}{dr} + C_x \frac{dC_x}{dr} + C_q \frac{dC_q}{dr} \quad (2.3)$$

From the thermodynamic relation, $Tds = dh - dp/r$, ignoring second-order terms

$$\frac{dh}{dr} = T \frac{ds}{dr} + \frac{1}{r} \frac{dp}{dr} \quad (2.4)$$

Substitution for dh/dr in equation (2.2), combining with the equation (2.1), will reduce to

$$\frac{dh_o}{dr} - T \frac{ds}{dr} = C_x \frac{dC_x}{dr} + C_q \frac{dC_q}{dr} + \frac{C_q^2}{r} \quad (2.5)$$

For the compressor, if the frequently used design condition of constant specific work at all radii is applied, then h_o will increase through the compressor in the axial direction, its radial distribution will remain uniform. Then equation (2.3) reduces to as follows.

$$C_x \frac{dC_x}{dr} + C_q \frac{dC_q}{dr} + \frac{C_q^2}{r} = 0 \quad (2.6)$$

As the density varies from hub to tip at the exit from the stators and the axial velocity is constant, integration over the annulus is necessary because of the continuity equation. Thus the following equation is used for the mass flow rate:

$$\dot{m} = 2\rho C_{x2} \int_{r_h}^{r_t} r_2 r dr \quad (2.7)$$

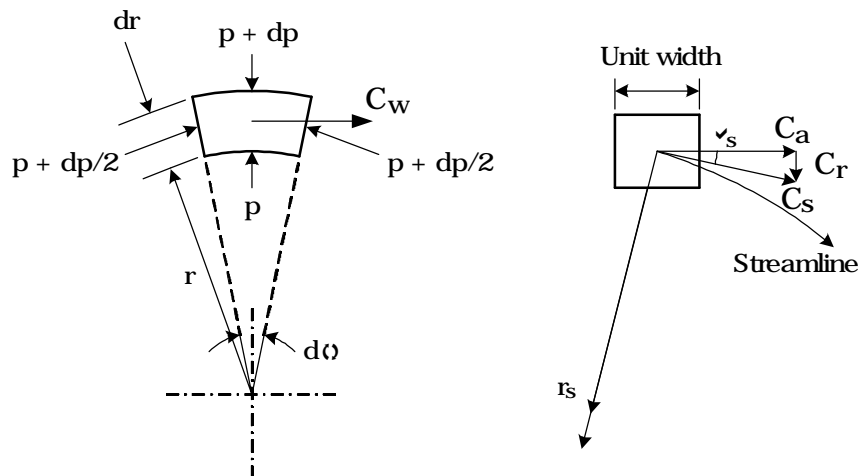


Figure 2.3 Radial equilibrium of fluid element

2.3 Meridional Flow Analysis for Turbines

The acceleration of a fluid particle at point P in the q direction may be written by [2]

$$\frac{DV_q}{Dt} = \frac{-V_q^2}{r} \sin(\mathbf{f} + \mathbf{a}) + \frac{V_m^2}{r_c} \sin \mathbf{a} + V_m \frac{dV_m}{dm} \cos \mathbf{a} \quad (2.8)$$

And the pressure gradient and component of blade force in the q direction are given by

$$-\frac{1}{r} \frac{dP}{dq} + F_q = \frac{DV_q}{Dt} \quad (2.9)$$

Consequently, the gradient of meridional velocity in the q-direction is as follows:

$$\begin{aligned} \frac{1}{2} \frac{dV_m^2}{dq} = \frac{dH}{dq} - T \frac{dS}{dq} - \frac{1}{2r^2} \frac{d(r^2 V_q^2)}{dq} - F_q \\ + \frac{V_m^2}{r_c} \sin \mathbf{a} + V_m \frac{dV_m}{dm} \cos \mathbf{a} \end{aligned} \quad (2.10)$$

The equation for the meridional velocity along the quasi-orthogonal line is solved in conjunction with the continuity equation for the mass flow across the quasi-orthogonal line AB. The mass flow is given by

$$\dot{m} = \int_A^B 2pr r V_m \sin \mathbf{a} dq \quad (2.11)$$

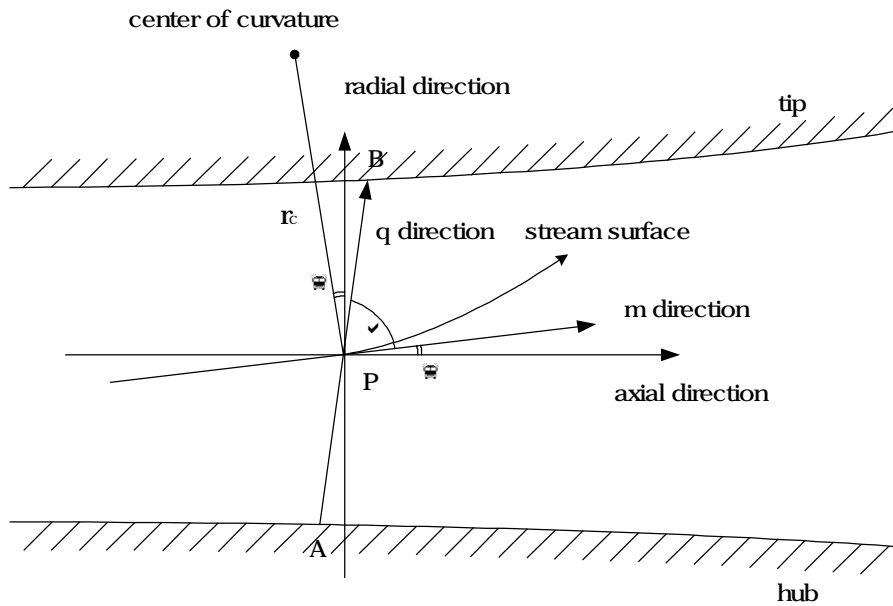


Figure 2.4 Geometry on a quasi-orthogonal

2.3 Estimation of stage performance

There are four kinds of primary sources of losses for compressors, namely the profile loss, the end-wall loss, the secondary loss, and the tip clearance loss. The loss models of Lieblein [3] and Koch-Smith [4] can be applied to estimate the compressor losses.

For turbines, the overall blade loss account for the four kinds of friction loss sources, namely the profile loss, the annulus loss, the secondary flow loss, and the tip clearance loss. The Ainley-Mathieson, Dunham-Came [5] and Moustapha-Kacker [6], and Kacker-Okapuu [7] models can be applied to estimate the turbine losses.

3. Results and Discussion

3.1 Design results of gas turbines

The high-pressure compressor and the high-pressure turbine are selected among the gas turbines because they are the representative components operated in severe conditions. The high-pressure compressor design data are summarized in Table 3.1. The low work coefficients were chosen in order to reduce the length of outer diameters.

Table 3.1 Design data of high-pressure compressor

Data	HP compressor
Number of stages	8
Mass flow rate (kg/s)	126.7
Rotational speed (rpm)	8000
Pressure ratio,	1.3201
Mean radius (m)	0.3810
First stage hub-to-tip ratio	0.8849
Last stage hub-to-tip ratio	0.9002
Average work coefficient	0.286
Mean flow coefficient	0.450
Shaft power (MW)	26.12
Total-to-total efficiency	90.21%

The comparison results of high-pressure compressor performance are summarized in Table 3.2.

Table 3.2 Performance comparison of high-pressure compressor

	MIT spec.	Results	Error
$P_{o,exit} / P_{o,inlet}$	1.32013	1.3201	-0.002%
$T_{o,exit} / T_{o,inlet}$	1.13096	1.131	0.004%
$h_{u,c}$	89.48%	90.21%	0.816%
W	26.1MW	26.12MW	0.077%

The meridional plane of the high-pressure compressor is shown in Figure. 3.1. And the flow properties are shown in Figures 3.2, 3.3, and 3.4. Figure 4.3 shows that the relative Mach number of the high-pressure compressor is in the range of 0.14~0.33. The Mach number is relatively high at the leading edge of the first stage rotor.

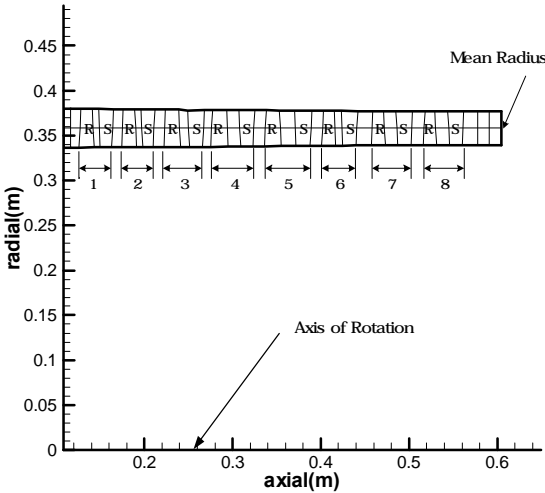


Figure 3.1 Meridional plane view of HPC

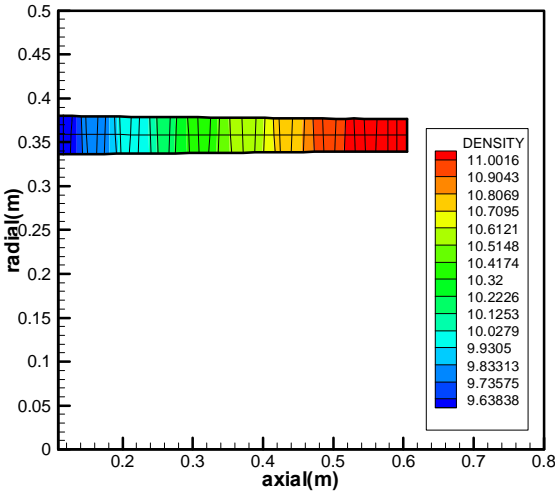


Figure 3.2 Fluid density of HPC

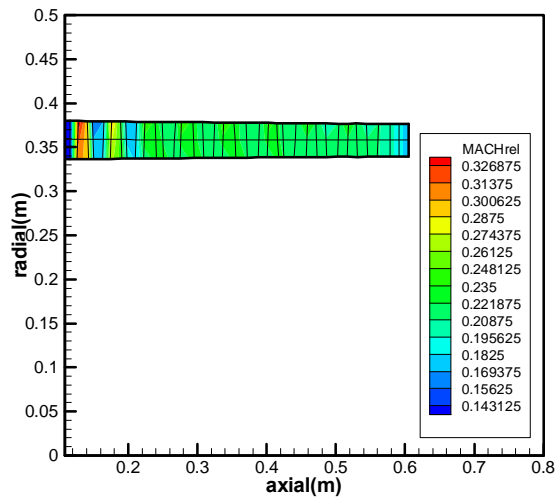


Figure 3.3 Relative Mach number of HPC

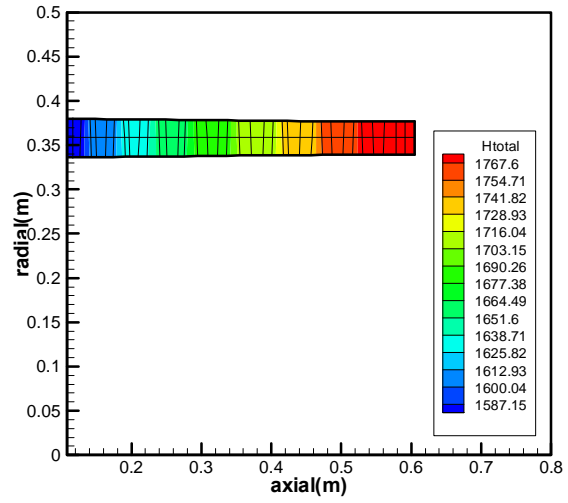


Figure 3.4 Total enthalpy of HPC

The high-pressure turbine design data are summarized in Table 3.3. Relatively high work coefficient and low flow coefficient were chosen in order to reduce the number of stages.

Table 3.3 High-pressure turbine design data

Data	HP turbine
Number of stages	4
Mass flow rate (kg/s)	126.7
Rotational speed (rpm)	8000
Pressure ratio	1.24243
Mean radius (m)	0.3400
First stage hub-to-tip ratio	0.7574
Last stage hub-to-tip ratio	0.7336
Average work coefficient	1.280
Mean flow coefficient	0.709
Shaft power (MW)	52.493
Total-to-total efficiency	92.24%

The comparison results of high-pressure compressor performance are summarized in Table 3.4.

Table 3.4 Performance comparison of high-pressure turbine

	MIT spec.	Results	Error
\dot{m}	126.7kg/s	126.383kg/s	-0.250%
$P_{o,inlet} / P_{o,exit}$	1.24224	1.24243	0.016%
$T_{o,inlet} / T_{o,exit}$	1.07479	1.07457	-0.020%
$h_{tt,t}$	92.24%	92.24%	0.000%
W	52.8MW	52.493MW	-0.581%

The meridional plane of the high-pressure turbine is shown in Figure. 3.5. And the flow properties are shown in Figures 3.6, 3.7, and 3.8. Figure 4.7 shows that the relative Mach number of the high-pressure turbine is in the range of 0.07~0.23. The Mach number is relatively high at the trailing edge of the fourth stage stator.

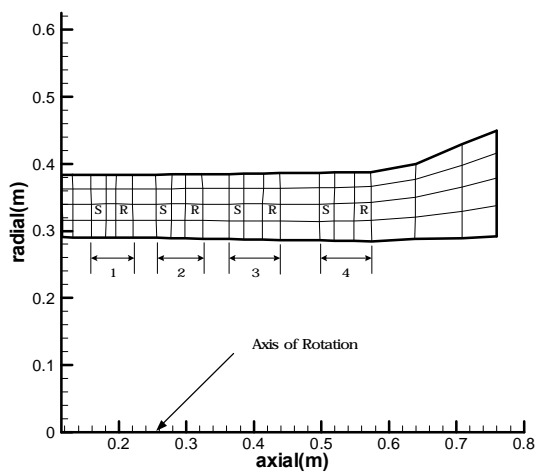


Figure. 3.5 Meridional plane view of HPT

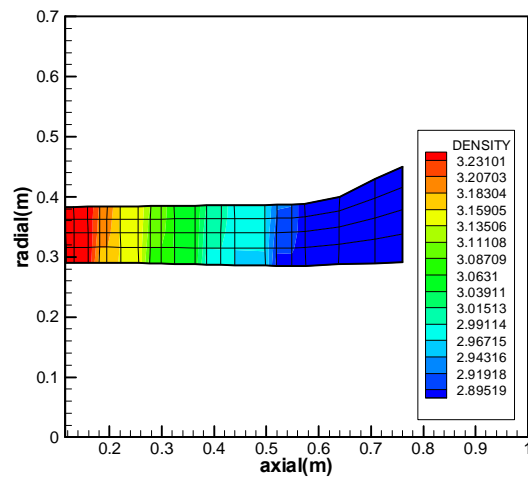


Figure 3.6 Fluid density of HPT

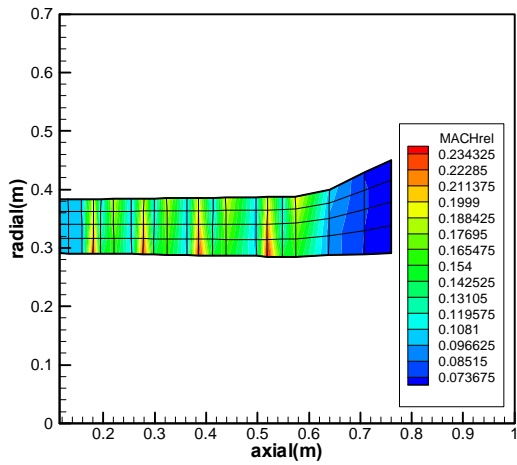


Figure 3.7 Relative Mach number of HPT

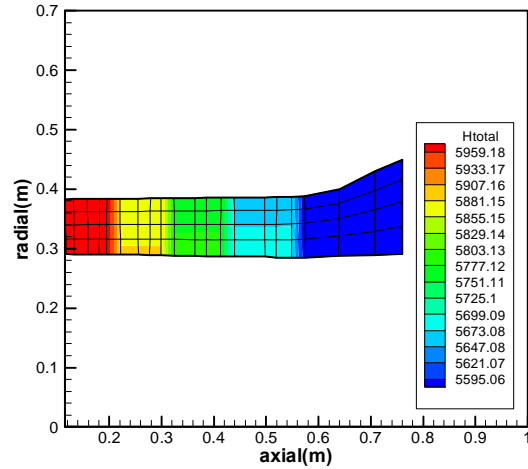


Figure 3.8 Total enthalpy of HPT

3.2 Off-design performance

The compressor characteristics were estimated using the de Haller number criterion, defined as $V_{ex}/V_{in} > 0.72$. Figure 3.9(a) shows the characteristic curves of the high-compressor expressed by plotting the stagnation pressure ratio against the non-dimensional mass flow for fixed values of the non-dimensional speed. And Figure 3.9(b) shows the characteristic curves expressed by plotting total-to-total stage efficiency against the non-dimensional mass flow for fixed values of the non-dimensional speed. Because of the relatively low flow coefficient, the constant rotational speed lines are not very steep as the mass flow rate increases. The efficiency decreases rapidly as the mass flow rate increases for fixed rotational speed.

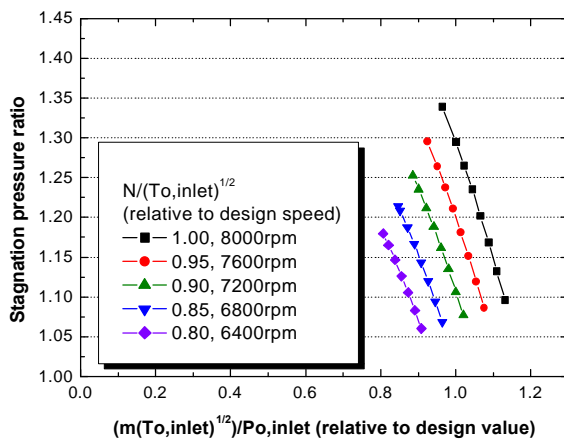


Figure. 3.9(a) HPC characteristics

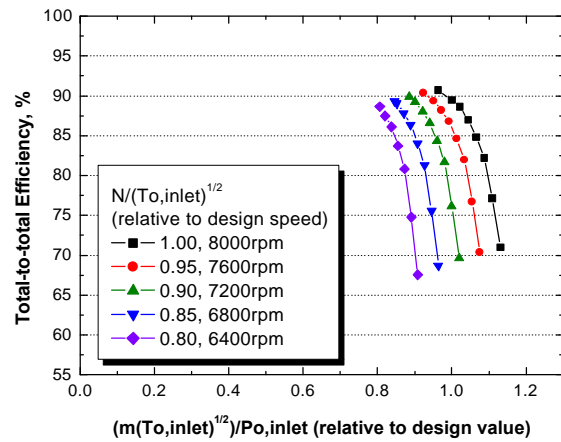


Figure. 3.9(b) HPC characteristics

Figure 3.10(a) shows that the characteristic curves of the high-pressure turbine are plotted by the non-dimensional mass flow against stagnation pressure ratio for various values of the non-dimensional speed. Figure 3.10(b) shows the characteristic curves expressed by plotting total-to-total stage efficiency against stagnation pressure ratio for various values of the non-dimensional speed. Because of the relatively high work coefficient, the efficiency decreases as the stagnation pressure ratio increases. The efficiency plot is relatively constant over a wide range of rotational speed and pressure ratio.

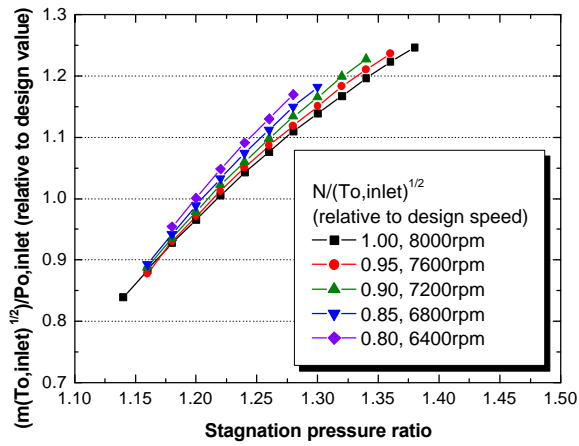


Figure. 3.10(a) HPT characteristics

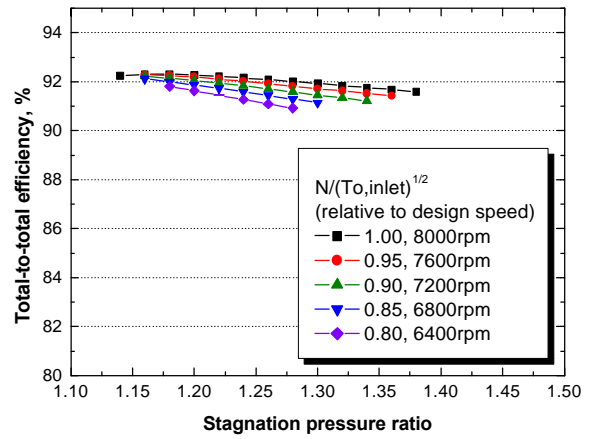


Figure. 3.10(b) HPT characteristics

3.3 Scaling Analysis

For geometrically similar machines with fixed gas conditions, taking non-dimensional groups yields

$$\frac{P_{o2}}{P_{o1}}, \frac{T_{o2}}{T_{o1}}, \mathbf{h} = f \left(\frac{\dot{m}\sqrt{T_{o1}}}{P_{o1}D^2}, \frac{ND}{\sqrt{T_{o1}}}, \frac{ND^2}{\mathbf{n}} \right) \quad (3.1)$$

Consequently, the gas turbine specifications should be corrected as mentioned above to present the performance relations. From the first group parameter condition for 1/2 scale gas turbines

$$(\dot{m})_{1/2scale} = 1/2(\dot{m})_{Full-scale}, \text{ and } (D)_{1/2scale} = 1/\sqrt{2}(D)_{Full-scale} \quad (3.2)$$

And from the second group parameter

$$N_{1/2scale} = \sqrt{2}N_{Full-scale} \quad (3.3)$$

However the last group cannot be duplicated exactly because of the difference of geometrical parameters:

$$\left(\frac{ND^2}{\mathbf{n}} \right)_{1/2\text{scale}} \neq \left(\frac{ND^2}{\mathbf{n}} \right)_{\text{Full-scale}} \quad (3.4)$$

Tables 3.7, 3.8, and 3.9 summarize the comparison results of 1/2 scaled high-pressure compressor, high-pressure turbine, and power turbine, respectively.

Table 3.7 Comparison between full-scale and 1/2 scale HPC performance

HP Compressor	Full-scale	1/2 scale	Error
P_{o2} / P_{o1}	1.3201	1.3201	0.000%
T_{o2} / T_{o1}	1.1310	1.1316	0.053%
$h_{tt,c}$	90.21%	89.63%	-0.643%

Table 3.8 Comparison between full-scale and 1/2 scale HPT performance

HP Turbine	Full-scale	1/2 scale	Error
P_{o1} / P_{o2}	1.24243	1.24241	-0.002%
T_{o1} / T_{o2}	1.07457	1.07459	-0.019%
$h_{tt,t}$	92.24%	92.24%	0.000%

4. Conclusions

In the present work, the conceptual design of axial flow gas turbines was performed for helium-cooled reactor. The specifications, the fluid properties through the turbomachines, the design point and the off-design performance were obtained on the basis of the mean-line design and the meridional flow analysis methods.

- (1) The conceptual design tools are capable of predicting design point performance with the range of $\pm 1\%$ error compared with the reference.
- (2) In the off-design characteristic curve, constant speed lines are not steep as the mass flow increases because the sonic velocity of helium is very high and low flow coefficient were chosen. The efficiency of the high-pressure was relatively constant over the wide range of pressure ratio.
- (3) The effect of the Reynolds number depends on the flow regime and it is significant to determine losses due to the boundary layer. In the subsonic flow, however, the effect of the Reynolds number is not large for 1/2 scale gas turbines and the scaling analysis indicates that the performance results of the scale-down models are quite similar to the full-scale data. The relative Mach number of the scaled gas turbine is below 0.34.
- (4) The overall results indicate that the helium gas turbine requires many stages for given temperature ratio or pressure ratio, and higher rotational speed and higher work coefficient can be chosen in order to bring the number of stages down because of the high sonic velocity of helium.

Nomenclatures

F_b	blade force
q	quasi-orthogonal distance
r_c	radius of curvature
C	absolute velocity
V	relative velocity
α	angle between q direction and axial direction
f	pitch angle between m direction and axial direction

References

- [1] H.I.H. Saravanamuttoo, G.F.C. Rogers and H. Cohen, "Gas Turbine Theory", Prentice Hall (2001)
- [2] J.D. Denton, "Throughflow Calculation for Transonic Axial Flow Turbines", Journal of Engineering for Power, Transactions of the ASME, Vol. 100, pp. 212-218 (1978)
- [3] Seymour Lieblein, "Loss and stall analysis of compressor cascades", Journal of Basic Engineering, Transactions of the ASME, pp. 397-400 (September 1959)
- [4] C.C. Koch and L.H. Smith, "Loss Sources and Magnitudes in Axial-Flow Compressors," Journal of Engineering for Power, Transactions of the ASME, pp. 411-424 (July 1976)

- [5] J. Dunham and P.M. Came, "Improvements to the Ainley-Mathieson Method of Turbine Performance Prediction," *Journal of Engineering for Power, Transactions of the ASME*, pp. 252-256 (July 1970)
- [6] S.H. Moustapha, S.C. Kacker and B. Tremblay, "An Improved Incidence Losses Prediction Method for Turbine Airfoils," *Journal of Turbomachinery, Transactions of the ASME*, Vol. 112, pp. 267-276 (April 1990)
- [7] S.C. Kacker and U. Okapuu, "A Mean Line Prediction Method for Axial Flow Turbine Efficiency," *Journal of Engineering for Power, Transactions of the ASME*, Vol. 104, pp. 111-119 (January 1982)